Inorganic Chemistry

Article

pubs.acs.org/IC

First-Principles Study of Microporous Magnets M-MOF-74 (M = Ni, Co, Fe, Mn): the Role of Metal Centers

Qiuju Zhang,[†] Baihai Li,[†,‡] and Liang Chen*[,†]

[†]Ningbo Institute of Materials Technology and Engineering, Chinese Academy of Sciences, Ningbo, Zhejiang 315201, People's Republic of China

[‡]Department of Materials Science and Engineering, University of Michigan, Ann Arbor, Michigan 48109, United States

Supporting Information

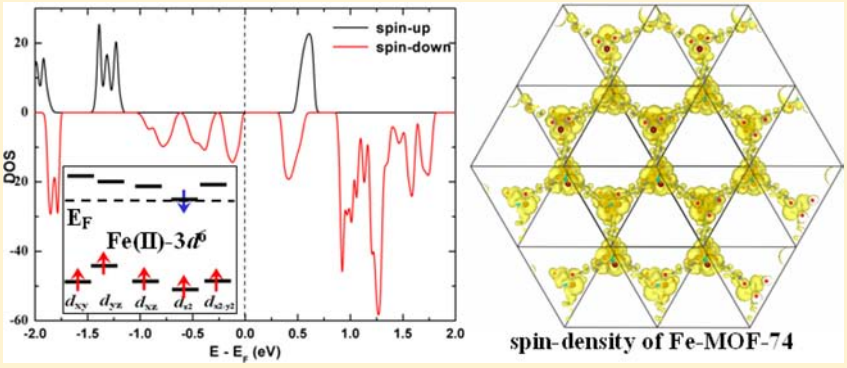

ABSTRACT: A clear understanding of the origin of magnetism in metal−organic frameworks (MOFs) would provide useful insight for tuning the electromagnetic properties of MOFs and finding new applications. In the present study, first-principles calculations show that the open paramagnetic metal sites in three-dimensional porous magnets M-MOF-74 (M = Ni, Co, Fe, Mn) favor high-spin electronic arrangement. Fe- and Co-MOF-74 exhibit ferromagnetic (FM) features and significantly distinct energy gaps between spin-up and spin-down channels in metastable states. After replacement of the Co center with a Ni ion, the FM feature was exhibited for the stable state since the "extra" valence electron was filled in the spin-down 3d bands to shift the Fermi level to higher energy. In contrast, after removal of one valence electron (i.e., replacement of the Fe center with Mn atoms), the energy gap was significantly enlarged and an antiferromagnetic (AFM) feature will be discerned.

INTRODUCTION

The development of porous magnetic materials has attracted a great deal of interest in the past decade.[1] It is anticipated that coupling the intrinsic magnetism and porosity within the same material will offer an ideal medium for applications in magnetic separation, magnetic sensing, or low-density magnets. Indeed, some recent reviews have already summarized the excellent advances that have been achieved to develop microporous magnetic solids. Among the most beautiful examples is the three-dimensional (3D) inorganic isostructural porous formates $M_3(HCOO)_6$, with M = Fe, Co, Ni, Mn. It is found that the magnetic ordering significantly relies on the paramagnetic metal centers in porous materials. Hence, iron, manganese, and nickel formates are ferromagnets, whereas the cobalt compound is a spin-canted antiferromagnet.[1d] Another example is that an Fe-doped Si nanotube has ferromagnetic (FM) coupling, while a Mn-doped Si nanotube prefers antiferromagnetic (AFM) coupling with a zero net moment.[2] In addition, some two-dimensional (2D) porous sheets (PSs) have also been predicted to exhibit magnetic behaviors by first-principles studies, e.g., the long-range ferromagnetism in a transition-metal phythalocyanine (TMPc; TM = Cr, Zn) single PS,[3] and FM half-metallicity in a dimethylmethylene-bridged triphenylamine PS.[4]

Metal−organic frameworks (MOFs) are one of the most important families of porous materials and have been extensively exploited in the application of gas storage, separation, and catalysis because of their extremely large surface area and porosity.[5] Beyond these applications, some MOFs also exhibit some unique magnetic properties;[6] e.g., one of the isomeric Fe^{II}-MOFs derived from isomeric ligands experiences a diamond-like 3D network spin-crossover to form a rare 2D hard ferromagnet.[6a] Another example is that Cu-MOFs derived from AFM dimeric Cu^{II} building units and nonmagnetic molecular linkers exhibit FM behavior, and copper vacancy would induce long-range FM ordering.[6h] Indeed, the huge structural variety of MOFs with paramagnetic TM ions offers a great opportunity to design desirable porous magnetic materials, such as low-density magnetic biomedicine, molecular magnets, and magnetic molecular sensors,[6h] beyond the traditional gas storage and separation. Particularly, under-

Received: April 15, 2013
Published: August 6, 2013

   dx.doi.org/10.1021/ic400927m | Inorg. Chem. 2013, 52, 9356−9362

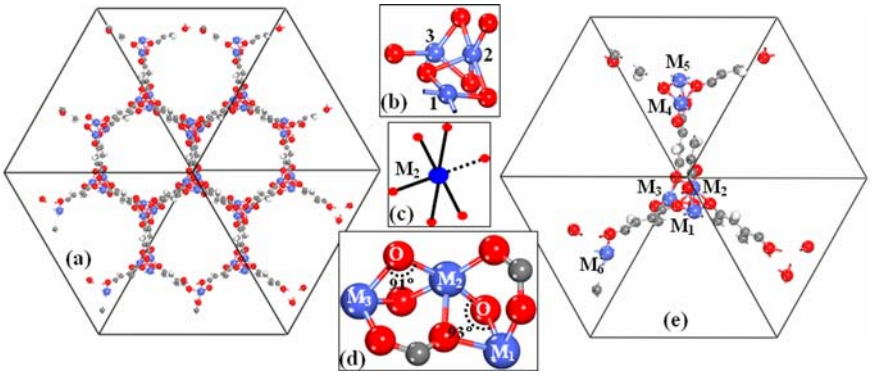

Figure 1. (a) Unit cell of M-MOF-74 repeated eight times, viewed from the [110] direction, showing the porous arrangement. (b) Coordination of the MO_5 fragment. (c) Square-pyramidal symmetry of the ligand field at the M site after removal of coordinated H_2O. (d) M−O−M connection to display the bonding angle. (e) One unit cell viewed along the [110] direction.

Table 1. Exchange Energy ($E_{ex} = E_{FM} - E_{AFM}$) between the FM and AFM States of M-MOF-74[a]

		M_{local}						
M-MOF-74	E_{ex} (eV)	M1	M2	M3	M4	M5	M6	M_{total} (μ_B)
M = Ni (FM)	−0.013	1.26	1.28	1.25	1.24	1.27	1.24	12.00
M = Co (FM)		2.62	2.62	2.62	2.62	2.62	2.62	18.00
M = Co (AFM_1)	0.033	2.61	−2.60	2.61	−2.61	2.62	−2.58	0.00
M = Co (AFM_2)	0.027	2.62	2.62	2.62	−2.62	−2.62	−2.62	0.00
M = Fe (FM)		3.74	3.74	3.74	3.74	3.74	3.74	24.00
M = Fe (AFM_1)	0.015	3.74	−3.72	3.72	−3.76	3.72	−3.73	0.00
M = Fe (AFM_2)	0.006	3.74	3.74	3.75	−3.75	−3.74	−3.74	0.00
M = Mn (AFM_1)	0.130	4.62	−4.62	4.62	−4.62	4.62	−4.62	0.00
M = Mn (AFM_2)	0.040	4.62	4.62	4.62	−4.62	−4.62	−4.62	0.00

[a]The M_{total} and M_{local} values for each ground state are listed to show their magnetic couplings. One exception is that M_{total} and M_{local} of metastable FM Co-MOF-74 are also presented because of its easily field-induced transition from the AFM state.

standing the magnetism of MOFs with open metal sites is important for tuning the magnetic properties of MOFs by host−guest interactions.[7]

Motivated by the manipulation of magnetic ordering with aforementioned TM-doping methods, we chose MOF-74 as the model system to study the electromagnetic behavior in MOFs by means of a density functional theory (DFT+U) method because isostructural MOF-74 containing various paramagnetic metal centers have been successfully synthesized.[8] In general, the DFT+U method could obtain qualitative improvement for the band gap and magnetic properties in the systems with strong electronic correlation between partially filled d shells. However, one limitation is that no value of U for M-MOF-74 based on firm experimental data could be obtained yet. Hence, we refer to U = 4 eV on the basis of a previous theoretical study of TMPc (TM = Cr, Mn, Fe, Co, Ni, Cu, Zn). For comparison and further evaluation of the U value, broader values of U = 2−8 eV have also been tested and a detailed description is presented in the next section.

■ COMPUTATIONAL METHOD

First-principles DFT calculations were performed to explore the magnetism in dehydrated M-MOF-74 (M = Ni, Co, Fe, Mn) using the Perdew−Burke−Ernzerhof generalized gradient approximation (PBE-GGA),[9] as implemented in the Vienna Ab-initio Simulation Package (VASP).[10] Because of the strong electronic correlation between partially filled d shells, standard GGA cannot present an accurate description for the electronic structure of M-MOF-74. In this regard, we employed the GGA+U method to obtain qualitative improvement for the band gap and magnetic properties.[11] On the basis of the previous study for TMPc (TM = Cr, Mn, Fe, Co, Ni, Cu, Zn) by Zhou and Sun,[3] the correlation energy (U) and exchange energy (J) were chosen to be 4 and 1 eV, respectively, for M-MOF-74 (M = Mn, Fe, Co, Ni) in this work. In addition, we have also tested U = 2−8 eV and found generally consistent magnetic and electronic properties for M = Mn, Fe, Co. One exception is that the electronic behavior of Ni-MOF-74 is dependent on the selection of U. No band gap is exhibited for U = 2−5 eV, while a significant band gap appears when $U \geq 6$ eV.

A plane-wave basis set was used to expand the Kohn−Sham orbitals with a kinetic energy cutoff of 400 eV within the PAW potential method.[12] A set of γ-centered k points (2 × 2 × 2) were used to sample the Brillouin zone in optimization,[13] while more accurate calculations within a 4 × 4 × 4 k mesh were performed to calculate the density of states (DOS). To model the dehydrated M-MOF-74, we applied one periodic unit cell containing 54 atoms, as shown in Figure 1. All lattice parameters and atomic positions were fully relaxed using the conjugated-gradient algorithm until the Hellmann−Feynman force on each atom was less than 0.03 eV/Å. The optimized lattice parameters are listed in Table S1 in the Supporting Information (SI).

To find the final stable state and spin alignments, different initial guesses were used for the local magnetic moments of the FM and AFM states (alternate up−down spins on TM atoms) for the four M-MOF-74 systems. To evaluate the possible effect of magnetic anisotropy and zero-field splitting (zfs) on the magnetic properties, the noncollinear calculations of the initial local magnetic moment along the x, y, and z directions and spin−orbital (SO) couplings are performed in Fe-MOF-74 as an example.

■ RESULTS AND DISCUSSION

AFM Coupling of M-MOF-74 (M = Co, Fe, Mn). The porous structures and their corresponding structural parameters of dehydrated M-MOF-74 are presented in Figure 1 and Table S1 in the SI, respectively. Each M atom is surrounded by five O

dx.doi.org/10.1021/ic400927m | Inorg. Chem. 2013, 52, 9356−9362

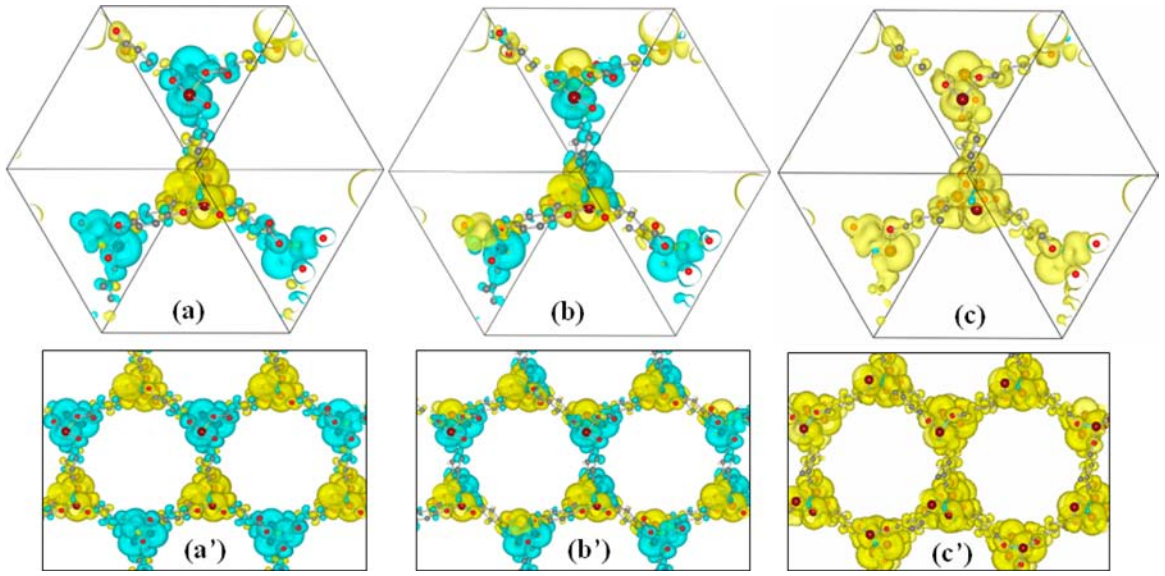

Figure 2. 3D spin density ($\rho\uparrow-\rho\downarrow$) with the isosurface at 0.5×10^{-3} e/A^3 for the two AFM and one FM states of Fe-MOF-74: (a and a′) spin densities for the unit cell and periodic pores for the AFM_1 model; (b and b′) spin densities for the unit cell and periodic pores for the AFM_2 model; (c and c′) spin density distributions on the unit cell and periodic pores for the metastable FM states. Yellow and blue contours illustrate the positive and negative spin densities.

atoms, i.e., one apical and four planar atoms, indicating a transformation from octahedral coordination to square-pyramidal coordination after removal of coordinated water molecules (Figure 1c). Such a transformation was also observed in the experimental study of Ni-MOF-74[14] and Co-MOF-74.[8c] The apical O atom forms a slightly longer M−O (e.g., Co−O) bond of 2.10 Å, compared to the four planar O atoms with Co−O bond lengths of 1.99−2.04 Å, which indicates that the fragment MO_5 is in distorted square-pyramidal coordination. The similar structural parameters of dehydrated Co-MOF-74 have also been obtained by Dietzel et al. upon performing an in situ high-temperature single-crystal experiment, where the Co−O distance at the apex of the pyramid (2.07 Å) is slightly longer than the other four Co−O distances in the range between 2.03 and 2.06 Å.[8c] The exchange energy E_{ex} ($E_{ex} = E_{FM} - E_{AFM}$) per unit cell in Table 1 can be used to identify the preferred magnetic coupling for each M-MOF-74 framework. It is found that FM coupling is only favorable in Ni-MOF-74 with E_{ex} = −0.013 eV/unit cell, while Fe-, Co-, and Mn-MOF-74 favor a weak AFM coupling with positive E_{ex} ranging from 0.006 to 0.130 eV/unit cell. Here we should emphasize that only two widely used AFM models were taken into account, yielding similar E_{ex} values. The model AFM_1 refers to the weak interchain AFM coupling and weak intrachain FM coupling, while the model AFM_2 refers to the alternative AFM coupling between adjacent metal centers. Actually, the model AFM_1 for both Co-MOF-74[8c]and Fe-MOF-74[6g] has been experimentally observed by Dietzel et al. and Bloch et al., respectively. The magnetic susceptibility measurements indicated a rather weak exchange energy J = 4.1 cm^{-1} (5×10^{-4} eV) for Fe-MOF-74, which is much smaller than our calculated E_{ex}. Such a difference is possibly attributed to the systematic error of the DFT method in the range of 0.01 eV, and therefore a quality evaluation is presented for calculation.

Because the electronic structures and particularly the magnetic properties are complicated by the presence of magnetic anisotropy, Fe-MOF-74 is taken as an example to evaluate the magnetic anisotropy by utilizing noncollinear calculations. Here, the initial local magnetic moments for each ion are given in the x, y, and z directions, respectively. As listed in Table S2 in the SI, $|E_{ex}| < 0.009$ eV/unit cell is not large for different magnetic directions. However, the local magnetic moments (M_{local}) of Fe atoms mainly distribute along the z direction and give rise to small projected $|M_{local}|$(Fe) < 0.099 μ_B in the x or y direction. Considering its Fe−O−Fe structure along the z direction, the magnetic anisotropy induced by the structure should be in existence in Fe-MOF-74. In addition, SO coupling is also calculated to estimate its effect on the magnetic properties because SO coupling often causes zfs. $|M_{local}|$ of each Fe ion is found to be about ±3.68 μ_B by considering SO coupling, which is only 0.06 μ_B smaller than the values of $|M_{local}|$ (Fe) = 3.74 μ_B obtained in the isotropic case. As expected, the zfs effect is weak in Fe-MOF-74 because SO coupling is not serious in 3d TMs.

To evaluate whether the magnetic ordering is long-range or not in the whole framework, we calculated and plotted the spin densities of the two AFM models of Fe- and Co-MOF-74, respectively. The obvious intrachain FM coupling and interchain AFM coupling can be discerned in the AFM_1 model in Figure 2a (a′) for the same blue or yellow spin densities distributed along each M−O−M chain direction. In contrast, alternative AFM coupling, which is represented by adjacent blue and yellow spin densities distributed in the same M−O−M chain [see Figure 2b (b′)], is noticed in the AFM_2 model. Most of the magnetic moments in Fe-MOF-74 are carried out by the central FeO_5 fragment, in line with our calculated larger M_{local} of ±3.74 μ_B on Fe cations. The neighboring C atoms on the hexagonal ring of the linker form much weaker M_{local} of no more than 0.16 μ_B. Thus, the overall spin-polarized electrons are connected through C−O−Fe fragments, which endows the whole framework with collective magnetic ordering. A similar spin-density distribution is also found in AFM Co-MOF-74 (Figure S1 in the SI), with M_{local} = ± 2.60 μ_B and zero total magnetic moment (M_{total}). The largest E_{ex} caused by Mn ions is well consistent with the previous study

dx.doi.org/10.1021/ic400927m | Inorg. Chem. 2013, 52, 9356−9362

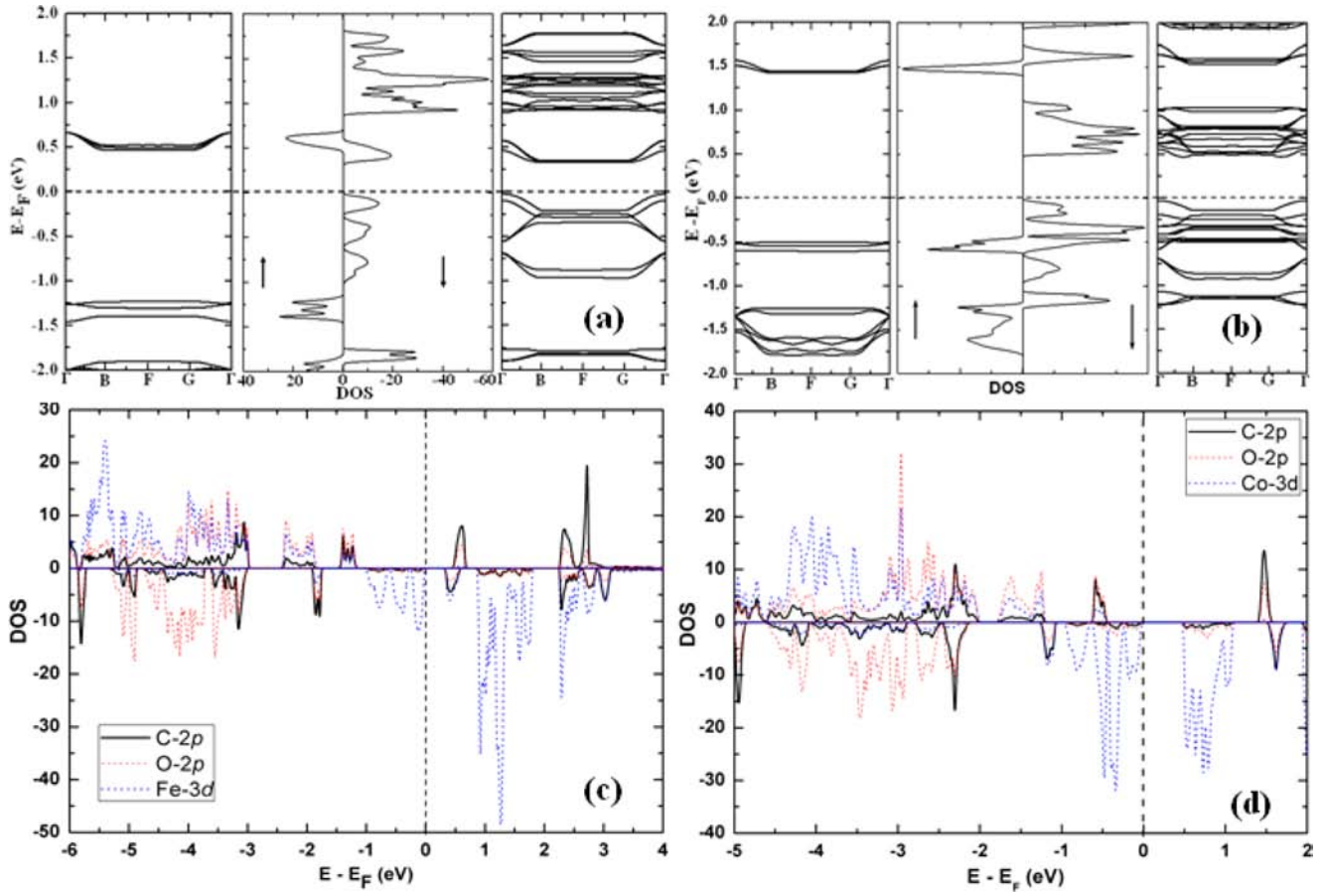

Figure 3. Spin-resolved TDOS, electronic band structures, and LDOS for FM Fe- and Co-MOF-74. The upper panels (a and b) are the calculated TDOS and the corresponding band structures to present the large different band gaps between the spin-up and spin-down components. The lower panels (c and d) are LDOS of C 2p, O 2p, and M 3d (M = Fe, Co), showing the main contributions of the VBM and CBM at the Fermi level.

that Mn-doped Pc has much higher E_{ex} (=0.124 eV) than Cr-, Fe-, Co-, and Cu-doped Pc.[3]

Metamagnetic States of FM Fe-MOF-74 and Co-MOF-74. We paid particular attention to the magnetic metastable (or "metamagnetic") states of FM Co- and Fe-MOF-74 because the transformation from AFM to FM has been experimentally induced by a weak magnetic field at above 8 K for Co-MOF-74.[8c] Such a transformation is in line with our calculated small E_{ex} values of 0.033 and 0.027 eV/unit cell for Co-MOF-74 and 0.0015 and 0.006 eV/unit cell for Fe-MOF-74 in the two AFM models. The total density of states (TDOS) and band structures showed that all spin symmetries were broken to yield large-spin splitting energies for FM Co- and Fe-MOF-74, as presented in Figure 3. Moreover, a very interesting phenomenon is discerned that the band gaps between the majority (spin-up) and minority (spin-down) components are significantly different. The spin-down DOS of Fe-MOF-74 (Figure 3a) and Co-MOF-74 (Figure 3b) exhibit narrow band gaps (E_g) of 0.30 and 0.49 eV, in sharp contrast to the much broader E_g values of around 1.75 and 2.00 eV for spin-up DOS.

In semiconductors, cavity electrons and itinerant electrons are the charge carriers, obtained by intrinsic excitation and closely related with E_g. Apparently, the smaller gap in the spin-down channel implies the probability to induce electron excitation from the valence band maximum (VBM) to the conduction band minimum (CBM) to filter a single spin-electron current. In the meantime, the spin-up channel is blocked because of the broader band gap. Such selective intrinsic excitation can possibly be induced by photoelectron irradiation with appropriate wavelength (λ). This property is analogous to half-metallicity observed in perovskite materials and TM-doped BN or Si nanotubes,[2,15] in which one spin component is metallic and the other one is semiconducting or insulating. Hence, if the narrow spin-down band gap is closed up by the semiconductive-metallic transition, the single spin-electron current in Fe- and Co-MOF-74 could also be filtered. We envisage that the readily induced single spin current may enable a potential application in spintronics.

The spin-resolved local density of states (LDOS) of C 2p, O 2p, and M 3d bands are plotted in Figure 3c,d to understand the origin of vastly different spin gaps in FM Fe- and Co-MOF-74. The spin-down VBM and CBM are clearly dominated by Fe 3d or Co 3d states at the Fermi level, indicating that the narrow gap is created by the split spin-down 3d states. In contrast, the spin-up VBM and CBM are mainly contributed by C 2p and O 2p orbitals located on the organic linkers. This broader gap is actually caused by the hybridization of C 2p and O 2p to form covalent C−O bonds because the hybridization would push the antibonding bands to higher-energy states and the bonding bands to lower-energy states. The overall positive spin densities obviously exhibited a FM coupling of intra- and interchains of FM Fe-MOF-74 [Figure 2c (c′)] and Co-MOF-74 (Figure S2 in the SI).

In nature, the magnetic moment originates from the unpaired electrons on each M ion, which is highly dependent on the high-spin (HS) or low-spin (LS) electronic configurations. It is

dx.doi.org/10.1021/ic400927m | Inorg. Chem. 2013, 52, 9356−9362

documented that the metal cations in MOF-74 are divalent ions, indicating that only 3d electrons participate in the magnetic ordering after the M ions (M = Mn, Ni, Fe, Co) lose all 4s electrons. Now we estimate the energy difference between the crystal-field splitting (Δ) and pairing energy to evaluate the overall stabilization energy for the HS and LS states. For an ideal square-pyramidal complex, the 5-fold degenerate 3d bands are split into four sub-bands: d_{xz} and d_{yz}, d_{xy}, d_{z^2}, and $d_{x^2-y^2}$. The split Fe and Co 3d LDOS in Figure 4 indicate that the crystal-field splitting for both metal centers is not significant with a moderate $\Delta \approx 1.5$ eV. In contrast, the spin-down components shift to much higher energy than spin-up components, so that strong spin splitting energies (δ) of 5.3 and 3.6 eV are induced for the Fe^{II} $3d^6$ and Co^{II} $3d^7$ bands, respectively. The larger δ would force the electrons not to pair up but spin parallel to each other, yielding a small pairing energy. According to Hund's rule and the Pauli exclusion principle, Fe^{II} $3d^6$ favors the HS state and nominally adopts the electronic configuration of $[(d\uparrow)^5(d_{z^2}\downarrow)^1]$, yielding four unpaired electrons (i.e., N_{ue} = 4). Similarly, Co^{II} $3d^7$ also prefers HS with the electronic configurations of $[(d\uparrow)^5(d_{z^2}\downarrow)^1(d_{x^2-y^2}\downarrow)^1)]$ and N_{ue} = 3. Such a HS arrangement (see the insets of Figure 4) and N_{ue} well rationalize the calculated M_{local} (2.60 and 3.74 μ_B) on each Co and Fe ion.

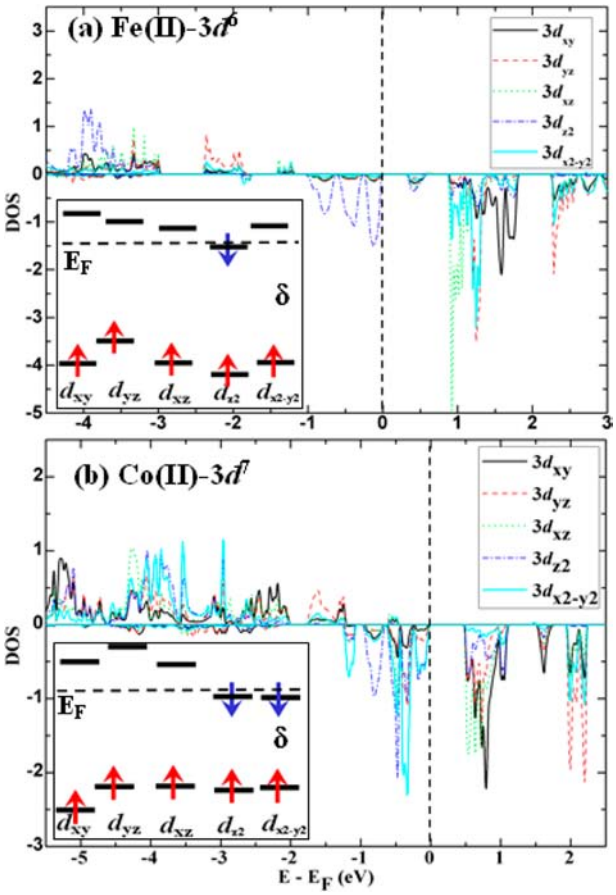

Figure 4. Spin-resolved LDOS of spin splitting for M^{II} 3d bands in FM states of Fe-MOF-74 (a) and Co-MOF-74 (b). The inset on each figure is the schematic illustration of electron configurations arranged in HS of Fe^{II} $3d^6$ and Co^{II} $3d^7$.

Transition from FM Ni-MOF-74 to AFM Mn-MOF-74. The electronic and magnetic properties are remarkably changed when a Mn^{II} or Ni^{II} ion is exchanged into the metal center, resulting in the transition from FM Ni-MOF-74 to AFM Mn-MOF-74. Indeed, the Ni^{II} ion has one more valence electron than the Co^{II} ion, which can be virtually regarded as the effect of "adding an electron". In contrast to the other three MOFs, Ni-MOF-74 exhibits the dependency of the band structures on the U values. The spin-resolved TDOS indicates that part of spin-down bands in Ni-MOF-74 cross the Fermi level and lead to zero band gap for U = 2−5 eV. For $U \geq 6$ eV, the band gap is enlarged to a significant value because the spin-up component near the Fermi level shifts to VBM. The magnetic ordering is still FM with M_{local} of 1.26 ± 0.02 μ_B and M_{total} of 12 μ_B. The spin-down VBM and CBM are dominated by Ni 3d bands, while the spin-up components are mainly composed of C 2p and O 2p bands. We should emphasize that the conductivity of Ni-MOF-74 is possibly very low because of the low concentration of charge carrier intrinsic to the localized 3d electrons, although the band gap is zero at U = 2−5 eV. However, a recently synthesized dimanganese (2,5-disulfhydrylbenzene-1,4-dicarboxylate) with infinite $(-Mn-S-)_\infty$ chains, also denoted as Mn_2(DSBDC), exhibits high intrinsic charge mobility.[16] As shown in the inset of Figure S4c in the SI, the larger Ni^{II} 3d splitting energy (δ = 2.8 eV) than the crystal-field-splitting energy ($\Delta \approx 0.8$ eV) indicates that Ni^{II} 3d also favors the HS state with five occupied spin-up 3d bands and three occupied spin-down 3d bands. The other two unoccupied spin-down bands contribute to the spin-down CBM.

In contrast, Mn-MOF-74 remarkably favors an AFM arrangement with a positive E_{ex} of 0.130 eV. The centered Mn^{II} ion has one less valence electron than the Fe^{II} ion, which leads to the half-filled $3d^5$ configuration. The spin-polarized TDOS (Figure 5a) and band structures (Figure S5 in the SI) clearly display a nearly symmetric feature in the spin-up and spin-down states, which produces an AFM semiconductor with $E_g \approx 1.55$ eV. To further elucidate the alternative AFM coupling in Mn-MOF-74, we plotted spin-resolved LDOS of Mn 3d bands for two adjacent Mn_1 and Mn_2 ions in Figure 5c. It can be seen that the spin-down 3d states of Mn_1 shift to higher energy above the Fermi level, whereas the situation is opposite for Mn_2 (i.e., spin-up 3d states shift to higher energy). Thus, the electronic configuration of Mn^{II} $3d^5$ has two half-filled states: all of the five electrons are filled in spin-up states (Mn_1) to produce positive M_{local} or all in spin-down states (Mn_2) to produce negative M_{local}, as depicted in Figure 5d. The corresponding alternate spin density of Mn-MOF-74 can be observed in Figure S6 in the SI. It is worth noting that the spin-splitting energy (δ = 7.8 eV) is the highest among the four MOF-74 frameworks, although adjacent Mn ions produce opposite spin splitting.

Apparently, the number of valence electrons and electronic configurations naturally determine the electronic and magnetic behaviors in M-MOF-74. HS arrangements are all favorable because of the much stronger spin splitting than crystal-field splitting in M 3d. N_{ue} arranged in HS electronic states has a well-defined linear relationship with M_{local} and M_{total} in M-MOF-74, as presented in Figure S7 in the SI. In FM Fe- and Co-MOF-74, the spin-down 3d bands are partially occupied. The filled electrons can readily transit between the close-lying occupied and unoccupied spin-down 3d bands, which yield relatively narrow E_g. For Ni-MOF-74, the more valence electrons in the Ni^{II} centers will slightly shift the Fermi level to higher energy states in order to complement more electron-filled 3d bands. Correspondingly, part of the spin-down bands

dx.doi.org/10.1021/ic400927m | Inorg. Chem. 2013, 52, 9356−9362

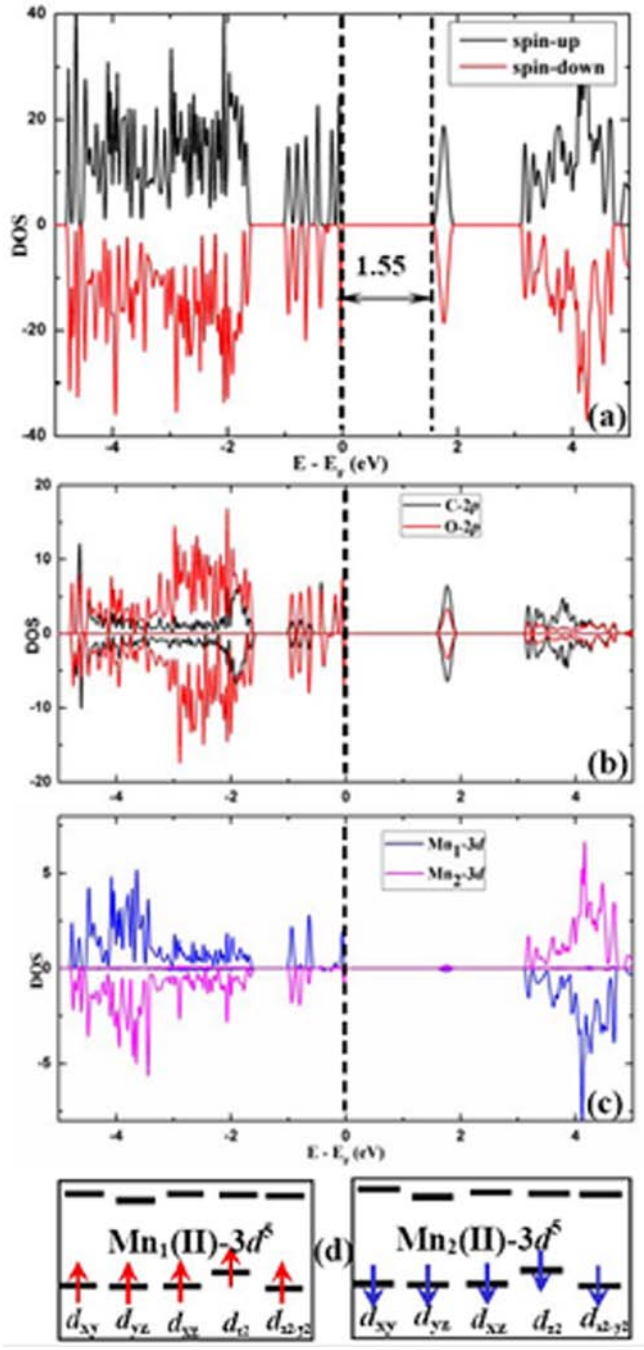

Figure 5. Spin-resolved TDOS and LDOS of AFM semiconducting Mn-MOF-74. (a) TDOS of Mn-MOF-74 displaying E_g = 1.55 eV at the Fermi level. (b) Decomposed C 2p and O 2p, illustrating the main components of VBM and CBM. (c) LDOS of 3d spin splitting for the adjacent Mn_1 and Mn_2 cations. (d) Two electron arrangements of Mn^{II} $3d^5$ with half-filled spin-up or spin-down 3d bands.

happen to cross the Fermi level and result in zero E_g at U = 2–5 eV. On the other hand, the half-filled Mn^{II} 3d with all spin-up electrons in Mn-MOF-74 eliminates the possibility of electron transition between spin-down bands. Furthermore, the large δ prohibits electron transition from spin-up to spin-down bands and, hence, results in broad gaps in both spins.

CONCLUSION

In summary, on the basis of spin-polarized DFT+U calculations, we have systematically investigated the electronic and magnetic properties of MOF-74 with different 3d metal centers. In the four MOF-74 frameworks, HS arrangements are all favored owing to the stronger 3d spin splitting than crystal-field splitting, which is the origin of their magnetism. The filling degree of spin-down bands determines the electron mobility and thus results in possible different electronic features for the four MOF-74 frameworks. Our studies may enhance the understanding of the origin of magnetism in MOFs and provide useful insight for tuning the electromagnetic properties of MOFs and designing low-magnetic materials.

ASSOCIATED CONTENT

Supporting Information

Structures and lattice parameters, spin densities of FM Co-MOF-74 and AFM Mn-MOF-74, spin-resolved TDOS and electronic band structures of Ni- and Mn-MOF-74, and linear relationship of M_{total}, M_{local}, and N_{ue} in FM M-MOF-74 (M = Ni, Co, Fe, Mn). This material is available free of charge via the Internet at http://pubs.acs.org.

AUTHOR INFORMATION

Corresponding Author

*E-mail: chenliang@nimte.ac.cn.

Notes

The authors declare no competing financial interest.

ACKNOWLEDGMENTS

We gratefully acknowledge helpful discussion with Prof. Jeffery Long, Prof. Shengbai Zhang, Prof. Guoqiang Liu, and Dr. Xiaobo Chen. We acknowledge financial support by the National Science Foundation of China (Grants 11274323 and 51272260), Science Technology Department of Zhejiang Province (Grant 2012C21108), and Innovative Research Project of Ningbo Municipal Government (Grants 2011B82005 and 2009B21005).

REFERENCES

(1) (a) Maspoch, D.; Ruiz-Molina, D.; Veciana, J. *J. Mater. Chem.* **2004**, *14* (18), 2713–2723. (b) Maspoch, D.; Ruiz-Molina, D.; Veciana, J. *Chem. Soc. Rev.* **2007**, *36* (5), 770–818. (c) Kuppler, R. J.; Timmons, D. J.; Fang, Q. R.; Li, J. R.; Makal, T. A.; Young, M. D.; Yuan, D.; Zhao, D.; Zhuang, W.; Zhou, H. C. *Coord. Chem. Rev.* **2009**, *253* (23–24), 3042–3066. (d) Dechambenoit, P.; Long, J. R. *Chem. Soc. Rev.* **2011**, *40* (6), 3249–3265.

(2) Singh, A. K.; Briere, T. M.; Kumar, V.; Kawazoe, Y. *Phys. Rev. Lett.* **2003**, *91* (14), 14682.

(3) Zhou, J.; Sun, Q. *J. Am. Chem. Soc.* **2011**, *133* (38), 15113–15119.

(4) Kan, E.; Hu, W.; Xiao, C.; Lu, R.; Deng, K.; Yang, J.; Su, H. *J. Am. Chem. Soc.* **2012**, *134* (13), 5718–5721.

(5) (a) Millward, A. R.; Yaghi, O. M. *J. Am. Chem. Soc.* **2005**, *127* (51), 17998–17999. (b) Zhou, W.; Wu, H.; Yildirim, T. *J. Am. Chem. Soc.* **2008**, *130* (46), 15268–15269. (c) Farrusseng, D.; Aguado, S.; Pinel, C. *Angew. Chem., Int. Ed.* **2009**, *48* (41), 7502–7513. (d) Zhang, Q.; Cao, L.; Li, B.; Chen, L. *Chem. Sci.* **2012**, *3* (9), 2708–2715. (e) Alapati, S. V.; Johnson, J. K.; Sholl, D. S. *Phys. Chem. Chem. Phys.* **2007**, *9* (12), 1438–1452. (f) Chen, Y.; Jiang, J. *ChemSusChem* **2010**, *3* (8), 982–988. (g) An, J.; Farha, O. K.; Hupp, J. T.; Pohl, E.; Yeh, J. I.; Rosi, N. L. *Nat. Commun.* **2012**, *3*, 604.

(6) (a) Li, L.; Clarkson, G. J.; Evans, D. J.; Lees, M. R.; Turner, S. S.; Scott, P. *Chem. Commun.* **2011**, *47* (47), 12646–12648. (b) Chen, M.

S.; Li, W.; Zhang, M. B.; Hu, R. X.; Zhang, C. H.; Chen, Z. M. *Z. Naturforsch., B: Chem. Sci.* **2011**, *66* (11), 1175−1178. (c) Tong, X. L.; Hu, T. L.; Zhao, J. P.; Wang, Y. K.; Zhang, H.; Bu, X. H. *Chem. Commun.* **2010**, *46* (45), 8543−8545. (d) Ryu, D. W.; Lee, W. R.; Lee, J. W.; Yoon, J. H.; Kim, H. C.; Koh, E. K.; Hong, C. S. *Chem. Commun.* **2010**, *46* (46), 8779−8781. (e) Mahata, P.; Sarma, D.; Natarajan, S. *J. Chem. Sci.* **2010**, *122* (1), 19−35. (f) Kurmoo, M. *Chem. Soc. Rev.* **2009**, *38* (5), 1353−1379. (g) Bloch, E. D.; Queen, W. L.; Krishna, R.; Zadrozny, J. M.; Brown, C. M.; Long, J. R. *Science* **2012**, *335* (6076), 1606−1610. (h) Shen, L.; Yang, S. W.; Xiang, S.; Liu, T.; Zhao, B.; Ng, M. F.; Goeettlicher, J.; Yi, J.; Li, S.; Wang, L.; Ding, J.; Chen, B.; Wei, S. H.; Feng, Y. P. *J. Am. Chem. Soc.* **2012**, *134* (41), 17286−17290.

(7) (a) Jesús, F. S.; Crespo, P. S.; Martijn, d. L.; Jorge, G.; Freek, K.; Miguel, J.; Joan, C.; Francesc, L.; Jorge, P. N.; Catalina, R. P. R.; Yves, J.; Emilio, P. *J. Am. Chem. Soc.* **2012**, *134*, 15301−15304. (b) Sun, Y. Y.; Kim, Y.-H.; Lee, K.; West, D.; Zhang, S. B. *Phys. Chem. Chem. Phys.* **2011**, *13* (11), 5042−5046. (c) Meilikhov, M.; Yusenko, K.; Torrisi, A.; Jee, B.; Mellot-Draznieks, C.; Poöpl, A.; Fischer, R. A. *Angew. Chem., Int. Ed.* **2010**, *49* (35), 6212−6215. (d) Jee, B.; Eisinger, K.; Gul-E-Noor, F.; Bertmer, M.; Hartmann, M.; Himsl, D.; Poöpl, A. *J. Phys. Chem. C* **2010**, *114* (39), 16630−16639.

(8) (a) Rosi, N. L.; Kim, J.; Eddaoudi, M.; Chen, B. L.; O'Keeffe, M.; Yaghi, O. M. *J. Am. Chem. Soc.* **2005**, *127* (5), 1504−1518. (b) Caskey, S. R.; Wong-Foy, A. G.; Matzger, A. J. *J. Am. Chem. Soc.* **2008**, *130* (33), 10870−10871. (c) Dietzel, P. D. C.; Morita, Y.; Blom, R.; Fjellvag, H. *Angew. Chem., In. Ed.* **2005**, *44* (39), 6354−6358.

(9) (a) Perdew, J. P.; Yue, W. *Phys. Rev. B* **1986**, *33* (12), 8800−8802. (b) Perdew, J. P. *Phys. Rev. B* **1986**, *33* (12), 8822−8824. (c) Lesar, R.; Herschbach, D. R. *J. Phys. Chem.* **1983**, *87* (25), 5202−5206. (d) Langreth, D. C.; Perdew, J. P. *Phys. Rev. B* **1980**, *21* (12), 5469−5493.

(10) (a) Kresse, G.; Hafner, J. *Phys. Rev. B* **1993**, *48* (17), 13115−13118. (b) Kresse, G.; Hafner, J. *J. Phys.: Condens. Matter* **1994**, *6* (40), 8245−8257. (c) Kresse, G.; Furthmuller, J. *Phys. Rev. B* **1996**, *54* (16), 11169−11186.

(11) Anisimov, V. I.; Aryasetiawan, F.; Lichtenstein, A. I. *J. Phys.: Condens. Matter* **1997**, *9* (4), 767−808.

(12) (a) Blochl, P. E. *Phys. Rev. B* **1994**, *50* (24), 17953−17979. (b) Kresse, G.; Joubert, D. *Phys. Rev. B* **1999**, *59* (3), 1758−1775.

(13) Monkhorst, H. J.; Pack, J. D. *Phys. Rev. B* **1976**, *13* (12), 5188−5192.

(14) (a) Dietzel, P. D. C.; Johnsen, R. E.; Fjellvag, H.; Bordiga, S.; Groppo, E.; Chavan, S.; Blom, R. *Chem. Commun.* **2008**, *41*, 5125−5127. (b) Dietzel, P. D. C.; Panella, B.; Hirscher, M.; Blom, R.; Fjellvag, H. *Chem. Commun.* **2006**, *9*, 959−961.

(15) (a) Xiang, H. J.; Yang, J. L.; Hou, J. G.; Zhu, Q. S. *New J. Phys.* **2005**, *7*, 39. (b) Nie, Y. M.; Hu, X. *Phys. Rev. Lett.* **2008**, *100* (11), 117023.

(16) Sun, L.; Miyakai, T.; Seki, S.; Dinca, M. *J. Am. Chem. Soc.* **2013**, *135* (22), 8185−8188.